

**CFD PREDICTION OF COUPLED RADIATION HEAT
TRANSFER AND SOOT PRODUCTION
IN TURBULENT FLAMES**

N. W. Bressloff, J. B. Moss and P. A. Rubini

School of Mechanical Engineering,
Cranfield University, Cranfield,
Bedfordshire, MK43 0AL, England.

Accepted for oral presentation at the *26th (Int.) Combustion Symposium*
in Naples, Italy, 1996.

Abstract

A novel coupled strategy is presented for predicting soot and gas species concentrations, and radiative exchange in turbulent combustion. The relatively slow processes governing soot formation are described by a model which accounts for radiative loss. In contrast to past studies, it is coupled here to the discrete transfer radiation model (DTRM) incorporating a weighted sum of gray gases (WSGG) solution to the radiative transfer equation, in an elliptic computational simulation. Incorporation of the WSGG solution in the DTRM provides a better representation of the non-gray radiative properties of combustion media than that offered by other more straightforward strategies, and without excessive computational expense. Combustion is modelled by an eddy breakup concept and the k-e turbulence model, with temperature evaluated from the solved enthalpy field. This complete strategy - the first reported of its kind - is applied to a confined turbulent jet diffusion flame burning methane in air. Confinement of the flame demands that account should be taken of the conjugate heat transfer at the boundaries. Numerical results are compared to experimental measurements of mixture fraction, temperature and soot volume fraction, and generally good agreement is achieved. Additionally, the computation of radiative exchange is considered in detail.

Introduction

Progress in the representation of increasingly complex combustion chemistry in CFD predictions of turbulent burning in engines, stationary powerplant and building fires has exposed significant shortcomings in the accompanying models of sooting processes and radiative heat transfer. Whilst laboratory scale flames burning hydrocarbon fuels with high H/C ratios at atmospheric pressure, are weakly sooting and optically-thin, most non-premixed burning in practical systems does not exhibit these characteristics. Uncertainties in computed gas temperatures of > 100 K associated with radiative exchange may then undermine much of the investment in extended reaction schemes, for example, for improved emissions prediction. The three-dimensional nature of most practical combustion geometries may impose additional constraints on the modelling approaches which may be usefully implemented in relation to the attainable resolution consistent with computational economy. The present study therefore develops a methodology which combines a laminar flamelet-based description of soot formation, an eddy breakup combustion model and radiative energy exchange by the discrete transfer method within the CFD framework of an elliptic flowfield calculation. The methodology is evaluated through detailed comparisons between CFD prediction and experimental measurement in a confined methane jet flame.

To date, essentially ad hoc representations of radiative heat loss have been employed in detailed predictions of turbulent flames - for example, in the form of perturbed state relationships, incorporated in fast chemistry/conserved scalar combustion models [1, 2], or approximate descriptions of radiative flux in the optically-thin limit, introduced into the balance equation for mean mixture enthalpy [3, 4] - but these admit only limited practical application.

The comparatively slow chemistry of soot formation requires that additional balance equations be solved for soot properties, whilst their strong temperature dependence insists that the influence of turbulent fluctuations also be accommodated in their averaged forms. The processes of soot formation and associated radiative heat loss are therefore closely coupled. A multiple flamelet approach, in which families of soot source terms, expressed as functions of mixture fraction, are distinguished by the degree of radiative loss experienced and averaged over the mixture fraction pdf [5], is here linked to an eddy breakup model of combustion heat release [6]. Thermal radiation is modelled using the discrete transfer radiation model [7] incorporating a weighted sum of gray gases solution to the radiative transfer equation [8]. This entails separate equations for each gray gas component with coefficients derived for mixtures of soot, CO₂ and H₂O [9]. Additionally, the formulation includes treatment of gray boundaries [10].

The complete strategy is evaluated by detailed comparison with measurements of mean mixture fraction, soot volume fraction and temperature in a confined turbulent methane jet flame. Whilst the present paper focuses on the integration of the several distinctive, but interacting model elements which make up the fully coupled calculation, a comparatively simple flame configuration has been adopted in order to provide a comprehensive data set for evaluation purposes.

Experimental Measurement

Detailed scalar measurements are reported in a co-flowing turbulent methane jet flame, confined within a cylindrical liner, by Brookes [11]. This confined flame configuration has also been employed in earlier sooting studies of prevaporised kerosine flames [12], to which reference should be made for general detail.

In the present application, methane issues from a cylindrical tube, 4.07 mm in diameter, at a flow rate of 10.3 g/min. The jet flame is rim stabilised by an annular premixed pilot flame. A co-flowing air stream occupies the remainder of the inlet contained within a pyrex cylindrical liner of 155 mm internal diameter. The overall equivalence ratio is 0.25.

Radial profiles of time-averaged mixture fraction, measured by microprobe sampling and mass spectrometric analysis, temperature by exposed bead, fine wire thermocouple and soot volume fraction by integrated laser absorption and tomographic inversion are reported at discrete flame heights of 150, 300, 350 and 425 mm.

Numerical simulation

Computational simulation is performed using a finite volume, general curvilinear CFD code called **SOFIE** (Simulation of Fires In Enclosures) currently being developed at Cranfield. A SIMPLEC pressure correction algorithm [13] for co-located velocities and pressure is used to evaluate the flowfield [14]. Momentum interpolation [15], and a second order TVD discretisation scheme [16] are employed to ensure a numerically stable solution without non-physical oscillations and false diffusion. The discretised equations are solved using a line-by-line tri-diagonal matrix algorithm. Further details of these techniques are available in the literature cited.

An important demand of numerical accuracy concerns the extent to which a converged solution is independent of the underlying grid. In the present study, 3600 internal flowing nodes are used in a prismatic sector of the axisymmetric geometry with mirror symmetry boundary conditions imposed on the two longitudinal faces thus produced. Finer resolutions yielded less than a 1% change in velocities and temperatures across radii at five distinct heights.

In common with previous studies of axisymmetric jet flames, a top-hat inlet profile is assumed with velocities of 20.16 and 0.61 ms^{-1} for methane and air, respectively. Although the flame is confined within a pyrex casing, which is itself contained inside a pressure vessel, only the inner flowfield is modelled. However, the internal face of the pyrex casing is treated as a conjugate heat transfer boundary condition. Additionally, the pyrex is assumed to be emitting as a gray surface ($\epsilon=0.8$), but no account is taken of the transmission properties of the material. Flowing boundaries are assumed to radiate as black bodies at the temperature of the adjacent gas.

Combustion model

Combustion is modelled by an eddy breakup concept such that fuel consumption is governed by the rate of mixing. Fast chemistry is assumed along with unity Lewis number and equal diffusivities of heat and mass. Chemical reaction occurs by a one-step mechanism in which fuel and oxidant react to generate a mixture of simple products. Separate balance equations are solved for mixture fraction and mass fraction of fuel. The mixing rate is predicted by a high Reynolds number k-e turbulence model [17] with modifications to the constants as recommended for confined, round turbulent jets [18].

Mass fractions of oxidant, diluent and products are determined directly from their respective state relationships. Combustion is coupled to all transported properties via the effect of heat release on temperature, and hence on radiative loss and density.

Energy conservation is represented by a balance equation for total enthalpy, which, in cartesian co-ordinates using tensor notation, is

$$\frac{\partial}{\partial x_j} (\bar{\rho} \tilde{u}_j \tilde{H}) = \frac{\partial}{\partial x_j} \left(\frac{\mu_{eff}}{\sigma_t} \frac{\partial \tilde{H}}{\partial x_j} \right) + \bar{S}_R \quad (1)$$

Total enthalpy is defined by

$$\tilde{H} = \sum \tilde{Y}_i (h_{f,i}^0 + \Delta \tilde{h}_i) \quad (2)$$

where $h_{f,i}^0$, $\Delta \tilde{h}_i$ and Y_i are the enthalpy of formation, the sensible enthalpy and the mass fraction of species i . Mean specific heat, c_p , is calculated from

$$c_p(\bar{T}) = \frac{\sum (\tilde{Y}_i c_{p,i}(\bar{T}))}{\sum \tilde{Y}_i / W_i} \quad (3)$$

where the individual molecular specific heats for CH₄, CO₂, H₂O, O₂ and N₂ are expressed as temperature polynomials [19]. The mean temperature, \bar{T} , is given by

$$\bar{T} = \frac{\sum \tilde{Y}_i (h_{f,i}^0 - c_{p,i}^*(\bar{T}_0))}{c_{p,i}^*(\bar{T})} \quad (4)$$

where $c_{p,i}^*(T)$ represents the integrated polynomials. Calculation of the radiative sink/source term, S_R , is described below. Radiative loss is manifested as a sink of energy, and thus reduces the energy available to increase sensible enthalpy (and temperature). This intimately linked equation set is closed by the calculation of density, which, for ideal gases is

$$\rho = P / R_0 T \sum \tilde{Y}_i / W_i \quad (5)$$

Soot prediction

As described in the introduction, an important feature of this work is the elliptic representation of radiation, and the coupling between radiative exchange and the concentrations of combustion products, especially soot. The kinetic processes governing soot formation - nucleation, surface growth and coagulation - are strongly dependent on temperature and density. Consequently, the prediction of soot volume fraction is very sensitive to radiative loss. The soot model is based upon solution of balance equations for soot number density, n , and soot mass concentration, f_v [20, 21]. To facilitate the representation of these quantities in Favre-averaged balance equations, n and f_v are replaced by $\phi_n = \frac{n}{\rho N_0}$ and $\phi_f = \frac{\rho_s}{\rho} f_v$, respectively; N_0 denotes Avogadro's number (6×10^{23}) and ρ_s signifies soot density (assumed to be 1800 kgm^{-3}). The equations are of the same form as Eq. (1) with total enthalpy replaced by either of ϕ_n or ϕ_f , and source terms given by [11]

$$S_n = a - \bar{\rho}^2 \bar{\beta} \bar{\phi}_n^{7/3} \bar{\phi}_f^{-1/3} \quad (6)$$

and

$$S_f = 8 + \bar{\rho} \bar{\gamma} \bar{\phi}_n^{1/3} \bar{\phi}_f^{2/3} \quad (7)$$

a and 8 represent the influence of nucleation on the number density and soot volume fraction, whilst $\bar{\beta}$ and $\bar{\gamma}$ characterise the processes of coagulation and surface growth, respectively. These soot formation parameters take the forms :

$$a = C_{\alpha} \rho^2 T^{1/2} X_F \exp(-T_{\alpha}/T) =: \delta/144$$

$$P = C_{\beta} T^{1/2}$$

$$\gamma = C_{\gamma} N_0^{1/3} \rho T^{1/2} X_F \exp(-T_{\gamma}/T)$$

such that each is modelled in terms of properties describable by state relationships. Consequently, mean values of the respective source terms are evaluated by integration over the local pdf of mixture fraction. Acetylene is used as the soot precursor, and the state relationship for the mass fraction of acetylene, X_F , is considered invariant with radiative loss. The coefficients, C_{α} , C_{β} and C_{γ} and activation temperatures, T_{α} and T_{γ} are determined by comparison between prediction and experimental measurement in laminar flames. They are [11]

$$C_{\alpha} = 6.54 \times 10^4 [m^3 / kg^2 K^{1/2} s],$$

$$C_{\beta} = 1.3 \times 10^7 [m^3 / K^{1/2} s],$$

$$C_{\gamma} = 0.1 [m^3 / kg^{2/3} K^{1/2} s],$$

$$T_{\alpha} = 46.1 \times 10^3 [K] \quad \text{and} \quad T_{\gamma} = 12.6 \times 10^3 [K]$$

A scheme has now been established to couple these source terms to the level of radiative loss [5]. The methodology is an extension of the laminar **flamelet** concept, which, in its standard form is unable to adequately represent finite rate chemistry by unique state relationships [4]. Here, a library of **flamelets** for enthalpy, temperature and density, are generated with each flamelet accounting for a different level of radiative loss. Then, by comparing the total enthalpy derived from solution of its balance equation with the

statistically integrated values obtained from the flamelet library, it is possible to determine which temperature and density flamelets are required to evaluate the parameters in the soot model. Statistical integration is performed with a β -function pdf determined from the Favre-averaged values of mixture fraction and its variance. Soot oxidation has not been included in the present work since uncertainties still attach to the representation of the mean source term in circumstances where the soot and oxidising species concentrations are highly correlated [5].

In the finite volume method, matrices generated by discretisation of the transport equations are "stiffened" if source terms become too large. As a consequence, converged solutions may not be achieved. In order to avoid such a scenario, source term linearisation is employed to the coagulation expression in Eq. (6).

Radiation model

Thermal radiation is modelled using the discrete transfer radiation model (DTRM). The DTRM employs a ray tracing procedure whereby the radiative transfer equation (RTE) is solved along paths representative of the angular discretisation of boundary cell faces. Consequently, radiative loss (or gain) of an individual control volume is evaluated as a balance between emission and absorption for all rays traversing that control volume. Summation of the final intensity at the end of a line of sight in all directions then yields the incident flux. For grey boundaries, the radiosity is represented by a combination of the emitted intensity and the reflected component of the incident intensity [7].

In typical engineering problems, the DTRM is weakened by the "ray effect" resulting from the finite angular discretisation of the solid angle hemisphere. The "ray effect" is exacerbated in axisymmetric geometries due to the failure of most rays to traverse regions close to the centre line. Unfortunately, a severe computational penalty is incurred by

using a very large number of rays in an attempt to overcome this. Alternative methods of discretisation are available which produce a more even distribution of rays [22]. In the present case, it is necessary to communicate information to and from the centreline of the axisymmetric geometry, without dramatically increasing the number of rays; thus, the original method of discretisation is modified so that a ray is always launched perpendicular to boundary faces. 129 rays are used in a compromise between accuracy and computational storage and speed.

One of the key attractions of the DTRM is the physically tractable representation of solution to the RTE. This feature of the method has been investigated elsewhere [10, 23] and good performance has been demonstrated for a weighted sum of gray gases solution to the RTE using coefficients to represent the radiative properties of CO₂-H₂O-soot mixtures. In this approach, the coefficients, $a_{m,n,n'}(T)$, k_n and $k_{n'}$ [9], normally employed to evaluate the total emissivity,

$$\varepsilon = \sum_{n,n'} a_{m,n,n'}(T) \left\{ 1 - \exp \left[-k_n [p_w + p_c] - k_{n'} \rho_s f_v \right] \right\} \quad (8)$$

are used to solve a separate transfer equation for each gray gas. p_w and p_c denote the partial pressures of H₂O and CO₂, respectively. The subscripts n and n' signify individual soot and gaseous components such that Eq. (8) reduces to the soot free and soot dominant limits. In the present paper, each pair of these values is represented by a single value, j , and the subscript m , denoting a mixture of soot and gas, is dropped. Solution of the RTE yields the intensity,

$$i_j = i_{0,j} \prod_{r=1}^N \tau_{j,r} + \sum_{r=1}^N \left[a_j i_{b,j,r} \epsilon_{j,r} \prod_{r'=r+1}^N \tau_{j,r'} \right] \quad (9)$$

for the j^{th} gas having traversed N elemental path lengths. Transmissivities, $\tau_{j,r}$, emissivities, $\epsilon_{j,r}$, and the black body intensity, $i_{b,j,r}$, are evaluated using mean properties across individual paths, assumed constant for each control volume. For black boundaries, the emitted radiation, $i_{0,j}$, is given by the black body intensity multiplied by the a_j coefficient, both evaluated at the boundary temperature [8]. When boundaries are gray, the inclusion of reflection demands a more detailed analysis. Separate expressions are required for the incident radiation of each grey gas, so that the reflected radiation in the individual transfer equations results solely from irradiation due to the same component. Therefore, at every boundary surface, for each grey gas, the incident intensity must be summed across all rays [10]. So, for gray boundaries, the initial intensity (denoted by subscript 0) of the j^{th} gray gas is

$$i_{0,j} = \frac{I}{\pi} \left[a_j(T_0) \epsilon_0 \sigma T_0^4 + [1 - \epsilon_0] \sum_{m=1}^M w_m i_{m,j} \right] \quad (10)$$

where a signifies the Stefan-Boltzman constant. The summation represents the total incident flux due to M rays for the j^{th} gas, with weightings, w , determined by the method of discretising the solid angle hemisphere [22]. This strategy is in contrast to the approach which solves a single RTE using total emissivities evaluated from Eq. (8) [24]. When gaseous radiation is significant, as in the case of methane, it is expected that the simpler

approach underestimates absorption, due to averaging of strong absorption in certain wavebands across the whole spectrum.

Evaluation of the radiative source term to the enthalpy equation in the DTRM is fairly straightforward, comprising summation of a weighted proportion of the intensity change of all rays traversing a control volume [7]. However, in the present study, it was found necessary to linearise the source term by expressing it explicitly as

$$S_R = L_1 - L_2 \bar{T}^3 \bar{T} \quad (11)$$

where, for the WSGG solution,

$$L_1 = \sum_{\text{all rays}} w \Delta A \sum_{j=1}^J [1 - \exp(-k_j l)] i_{n-1} \quad (12)$$

$$L_2 = \frac{\sigma}{\pi} \sum_{\text{all rays}} w \Delta A \sum_{j=1}^J \pi_j(\bar{T}) [1 - \exp(-k_j l)] \quad (13)$$

The first order temperature in Eq. (11) is then expressed in terms of total enthalpy. The term, i_{n-1} , represents the intensity of a ray as it arrives at a control volume, and ΔA signifies the area of the boundary face from which the ray originates.

Results and Discussion

Predicted radial variations of mixture fraction and temperature are compared against experiment at heights of 150, 300 and 425 mm in Figs. 1 and 2, respectively. The agreement for mixture fraction is generally good (cf. Fig. 1). There is some uncertainty

F; 1

relating to mixture fraction measurements by probe sampling in leaner regions at the edges of sooting flames due to carbon retained in the sampling lines. Nonetheless, mixing is comparatively poorly modelled there, and this is reflected in both the computed mixture fraction profiles, and in the slower spreading of the temperature predictions shown in Fig. 2. Again, at heights of 150 and 300 mm, temperature is well predicted, particularly in terms of the negative gradient. Differences of less than 10 % are observed along the axis, and the maxima are captured with superior accuracy. Similar performance prevails close to the centre line at a height of 425 mm, but spreading of the flame is less well represented with temperature predictions falling significantly below the measured values. Since a similar spreading deficiency was observed for an adiabatic flame calculation, we have concluded that both the present implementation of the k-e model, and the simplified representation of chemical reaction, are largely responsible for this poor performance.

Due to the weakly sooting nature of methane-air flames at atmospheric pressure, combined with the difficulty of accurately recording low levels of soot concentration, measurements of soot volume fraction were only performed at heights of 300, 350 and 425 mm above the inlet. Radial variations at these heights are compared in Fig. 3. The numerical predictions are expected to be somewhat greater than the measured values due to the exclusion of oxidation from the soot model. Nonetheless, the key trends in the evolution with downstream distance are captured by the computed profiles. Even in the absence of oxidation, the rate of increase of centre line soot concentration is reduced as the mixture fraction (and fuel concentration) falls.

The coupling between radiation and soot formation in the present configuration can only be expected to demonstrate discernible interaction close to the centre line, in regions where there are significant levels of soot. Even there, the presence of relatively high concentrations of CO_2 and H_2O will tend to dominate the radiative effects of the gas-soot

mixture [23]. These characteristics are clearly represented in Fig. 4 which shows the radiative exchange at heights of 150 and 300 mm. A comparison is made between the output from the predicted gas-soot mixture, and the output when soot is neglected. In both cases, maximum radiative loss occurs at a height of approximately 300 mm, and at a radius of almost 20 mm. Although it is physically unrealistic to view net radiative exchange as a linear combination of that due to individual components, the adjustment for overlap is relatively small. Consequently, it is reasonable to describe the loss from the mixture at 150 mm as being only slightly greater than for gases alone. By 300 mm the soot contribution has become more significant as concentrations approach 0.1 ppm. The molar fractions of CO_2 and H_2O at this height are approximately 0.08 and 0.16, respectively.

Fig. 4

Paradoxically, both soot and gas species concentrations, and temperature are maximised further downstream than the 300mm height. It must be emphasised, however, that radiative exchange is a balance between emission and absorption. Although higher concentrations and temperature may produce greater emission at one location rather than another, increased absorption in neighbouring regions can result in lower net radiative loss.

The oscillating nature of radiative exchange is a feature of the "ray effect". Within the constraints imposed by computational memory and speed, these oscillations are damped to an acceptable level by using 129 rays per boundary face. It is also to be noted that the balance between radiative loss and the total radiative flux at boundaries, for this number of rays, differed by approximately 7 %. When 65 rays were used in the same calculation, an almost identical balance was obtained. However, unacceptably large oscillations were produced in the radiative source term distribution.

With respect to the overall energy balance, an error of less than 1 % exists on this 3600 node grid using 129 rays. Within the computational domain, over 99 % of the available chemical energy is released by the time the flow reaches a height of 425 mm. For the flow conditions analysed here, this represents an energy flow rate of approximately 740 J/s. Of this, over a third is radiated to the boundaries. The radiative loss from methane-air flames is normally about 20 % [25], but this factor is augmented in our case due to higher temperatures accompanying confinement of the flame.

Finally, an important feature affecting convergence rates concerns the frequency at which the radiation algorithm is called relative to the main CFD routine. Early in the calculation, a low frequency is acceptable, but eventually this has a deleterious effect on convergence as a large perturbation is inflicted on the enthalpy equation. It is not necessary, however, to recalculate the radiative field with every CFD iteration; indeed, such an approach is exhaustive. A compromise adopted in this analysis is to call the radiation algorithm after 20 CFD iterations. On a DEC Alpha 200 4/100 workstation, the CFD and radiation algorithms require 3.3 and 103.2 seconds of cpu time per iteration, respectively.

Conclusions

A general strategy has been described for the prediction of turbulent non-premixed hydrocarbon combustion which combines modelling of finite rate soot formation, sensitive to the influence of turbulent scalar fluctuations, with a simplified representation of combustion heat release and detailed solution of the accompanying coupled equation of radiative exchange.

The effect of radiative loss on the temperature-dependent chemistry of soot nucleation and surface growth is accommodated through an extended flamelet approach.

Radiative exchange is computed using the discrete transfer radiation model with properties established from the local mean concentrations of CO_2 , H_2O and soot. A weighted sum of grey gases solution to the radiative transfer equation is employed, including interaction with gray boundaries. The coupled solution for radiative exchange, even for this comparatively weakly sooting fuel, reveals the importance of both absorption and emission within the turbulent flame zone.

Detailed comparisons between prediction and experiment in a confined methane jet flame for the critical properties mixture fraction, soot volume fraction and temperature demonstrate the effectiveness of the approach within an elliptic flowfield calculation. Therefore, extension to more complex geometries of the finite volume CFD approach and the accompanying sub-models as described herein, is now envisaged. With the aid of embedded grids, it will be possible to accurately resolve the characteristics of a combustion source, without demanding unfeasible computer resources, as would be required if the same grid resolution were employed throughout the computational domain.

Acknowledgements

The authors are pleased to acknowledge the contribution of Steven Brookes, in particular, in making available his property measurements in the methane jet flame, and of EPSRC through the award of the research grant under which this study was undertaken.

References

1. Crauford, N. L., Liew, S. K. and Moss, J. B., *Comb. Flame* 61, p. 63, 1985.
2. Fairweather, M., Jones, W. P., Ledin, H. S. and Lindstedt, R. P., *Twenty-fourth Symposium (International) on Combustion*, p. 1067, Combustion Institute, 1992.
3. Faeth, G. M., Jeng, S-M. and Gore, J. P., *Heat transfer in Fire and Combustion Systems*, HTD 45, p.137, ASME, 1985.
4. Kent, J. H. and Honnery, D., *Combust. Sci.Tech.*, 54, p. 383, 1987.
5. Young, K. J. and Moss, J. B., *Combust. Sci. Tech.*, 105, p. 33, 1995.
6. Magnussen, B. F. and Hjertager, B. H., *Sixteenth Symposium (International) on Combustion*, p. 719, Combustion Institute, 1976.
7. Lockwood, F. C. and Shah, N. G., *Eighteenth Symposium (International) on Combustion*, p. 1405, Combustion Institute, 1981.
8. Modest, M. F., *J. Heat Transfer*, 113, p. 650, 1991.
9. Truelove, J. S., *HTFS DR33*, AERE, Harwell, Oxon, England, 1975.
10. Bressloff, N. W., Moss, J. B. and Rubini, P. A., Assessment of a Differential Total Absorptivity Solution to the Radiative Transfer Equation as Applied in the Discrete Transfer Radiation Model, *Numerical Heat Transfer*, accepted for publication, 1996a.
11. Brookes, S. J., Coupled Soot Production and Thermal Radiation from Turbulent Jet Flames, Ph.D.Thesis, Cranfield University (in preparation, 1996).
12. Young, K. J., Stewart, C. D. and Moss, J. B., *Twenty-fifth Symposium (International) on Combustion*, p. 609, Combustion Institute, 1994.
13. Patankar, S. V., *Numerical Heat Transfer and Fluid Flow*, Hemisphere Publishing Corp., 1980.
14. Melaaen, M. C., *Num. Heat Trans.*, Part B, Vol. 21, p. 1, 1992.
15. Majumdar, S., *Num. Heat Trans.*, Vol. 13, p. 125, 1988.

16. van Leer, B., *J. Comput. Phys.*, Vol. 14, p. 361, 1974.
17. Launder, B. E. and Spalding, D. B., *Mathematical Models of Turbulence*, Academic Press, 1972.
18. Rodi, W., *Ph.D. Thesis*, University of London, UK, 1972.
19. McBride, B. J., Gordon, S. and Martin, A. R., *NASA TM4513*, 1993.
20. Moss, J. B., Stewart, C. D. and Syed, K. J., *Twenty-Second Symposium (International) on Combustion*, The Combustion Institute, p. 413, 1988.
21. Syed, K. J., Stewart, C. D. and Moss, J. B., *Twenty-Third Symposium (International) on Combustion*, The Combustion Institute, p. 1533, 1990.
22. Bressloff, N. W., Moss, J. B., Rubini, P.A., *3rd European Conference on Industrial Furnaces and Boilers*, Lisbon, Portugal, 1995.
23. Bressloff, N. W., Moss, J. B. and Rubini, P. A., The Differential Total Absorptivity Solution to the Radiative Transfer Equation for Mixtures of Gases and Soot, submitted for publication to *Numerical Heat Transfer*, 1996b.
24. Abbas, A. S. and Lockwood, F. C, *Twenty-first Symposium (International) on Combustion*, The Combustion Institute, p. 285, 1986.
25. Jeng, S-M. and Faeth, G. M., *J. Heat Trans.*, Vol. 106, p.886, 1984.

List of Figures

1. Radial variation of mean mixture fraction at heights of 150, 300 and 425 mm above the inlet.
2. Radial variation of mean temperature at heights of 150, 300 and 425 mm above the inlet.
3. Radial variation of mean soot volume fraction at heights of 300, 350 and 425 mm above the inlet.
4. Comparison between radiative exchange due to soot-CO₂-H₂O and CO₂-H₂O mixtures at heights of 150 and 300 mm.

Figure 1

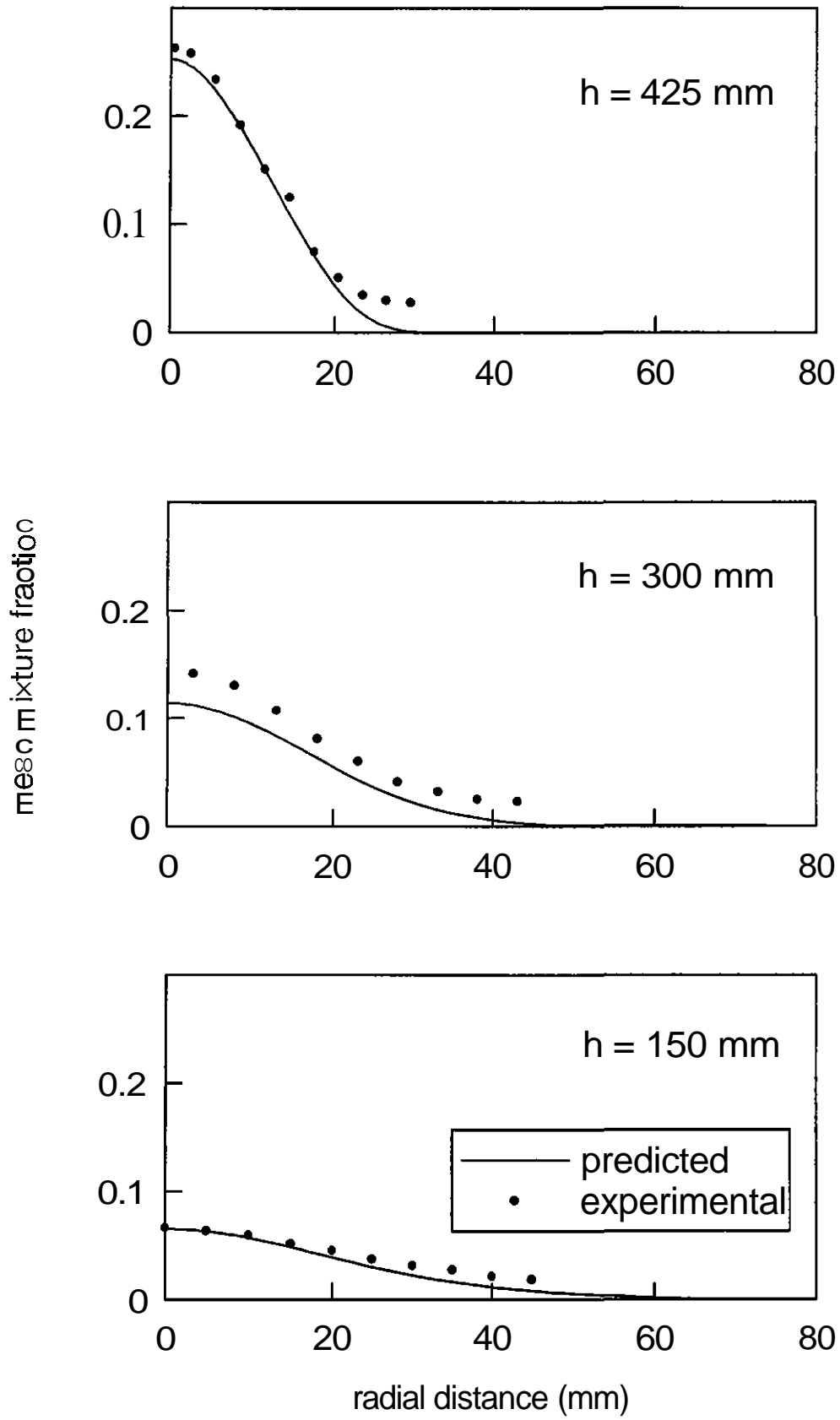


Figure 2

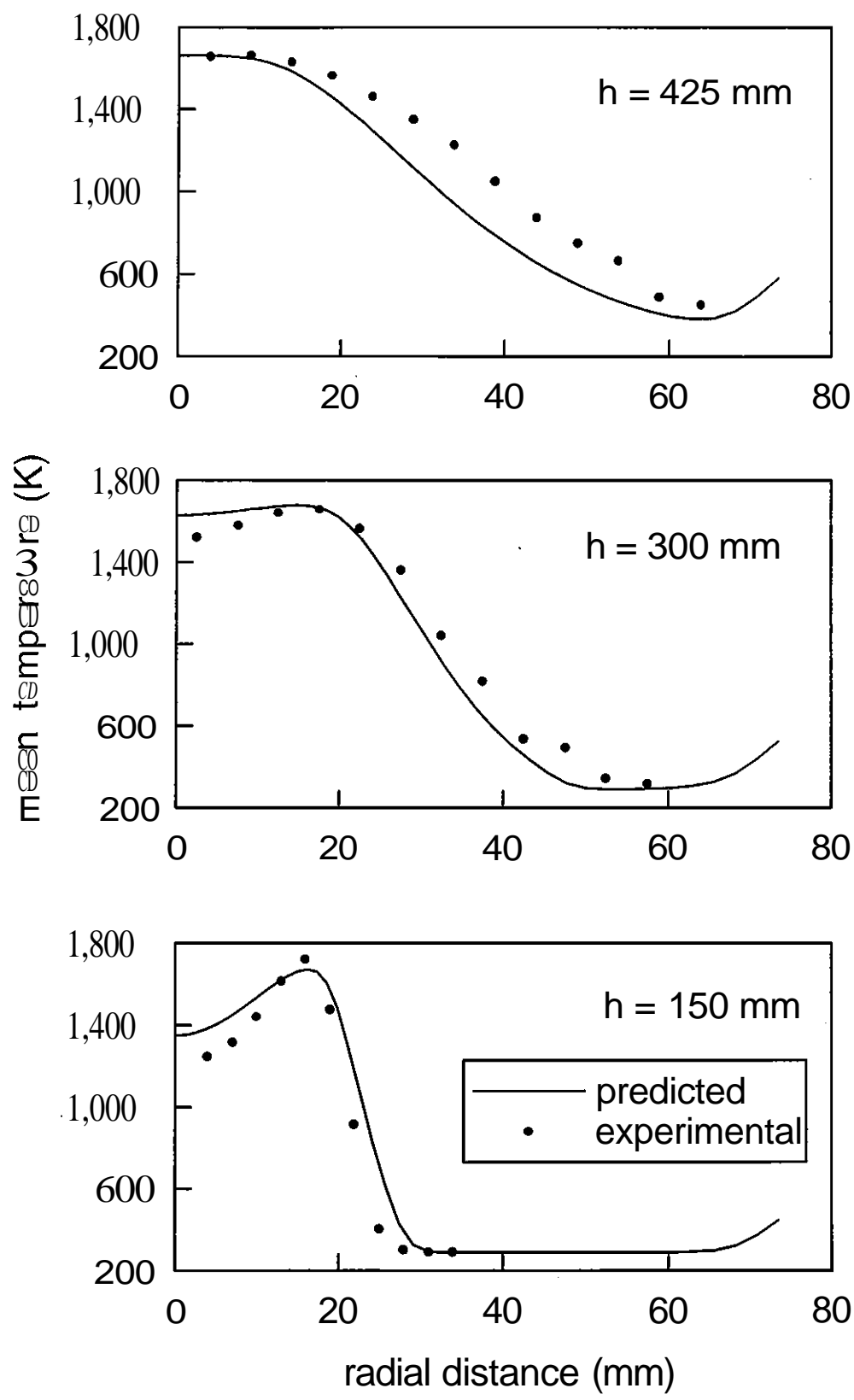


Figure 3

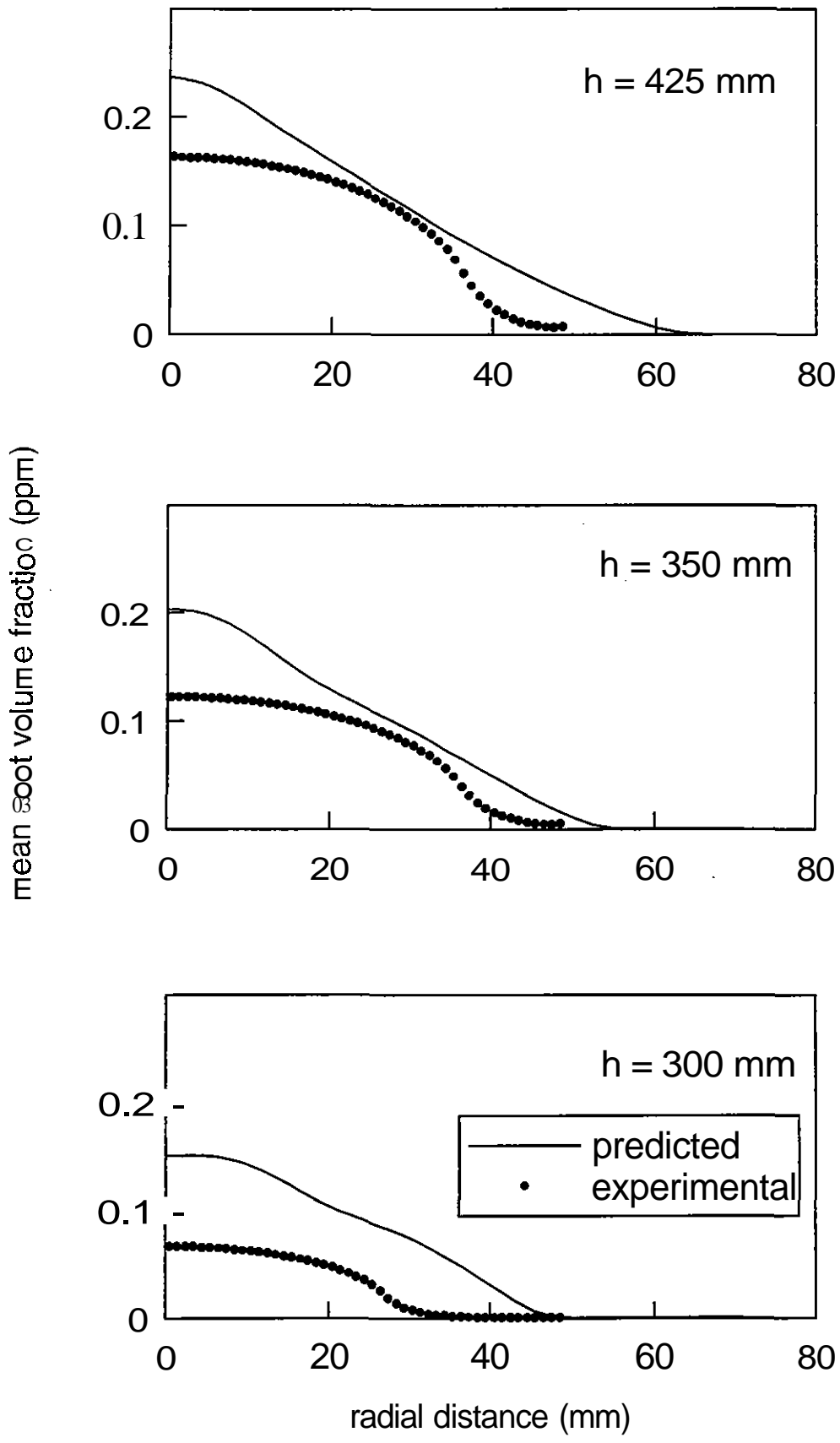


Figure 4

